Available online at www.sciencedirect.com
SCIENCE DIRECT®
Chemical Physics 300 (2004) 53–62
Chemical Physics
www.elsevier.com/locate/chemphys

Volumetric and infrared measurements on amorphous ice structure

C. Manca [a], C. Martin [b], P. Roubin [b,*]

[a] Institut für Chemie und Biochemie, Universität Bern, Freiestrasse 3, 3000 Bern 9, Switzerland
[b] Laboratoire Physique des Interactions Ioniques et Moléculaires UMR 6633, Université de Provence, Centre Saint-Jérôme (service 242), F-13397 Marseille Cedex 20, France

Received 30 July 2003; accepted 6 January 2004

Abstract

We have simultaneously used adsorption isotherm volumetry and Fourier transform infrared spectroscopy in order to take the investigations on amorphous ice structure a step further, especially concerning porosity and annealing-induced modifications. We have studied surface reorganization during annealing and found that the number of surface sites decreases before crystallization, their relative ratios being different for amorphous and crystalline ice. We also present results confirming that ice can have a large specific surface area and nevertheless be non-microporous.

Keywords: Adsorption isotherm; Infrared spectroscopy; Amorphous ice; Surface sites; Porosity

1. Introduction

The knowledge of amorphous ice structure has focused attention for several decades since it is one of the most abundant components in the interstellar medium [1–4]; the goal is to understand its role in interstellar chemistry and in formation of large organic compounds [5–10]. Amorphous ice is not stable under the temperature and pressure conditions of earth, and this is why many researchers have tried to establish processes to obtain amorphous ice. It can be formed by (i) submitting crystalline ice to a pressure higher than 10 bar at 77 K [11]; (ii) rapid cooling of small drops of water [12]; (iii) condensing water vapor on a cold substrate [13–18]; (iv) the same as (iii) using a carrier gas at a temperature high enough to prevent its crystallization [19]. The last two methods are the most widely used, and the experimental conditions of ice formation such as the condensation rate [4,14,20], the deposition temperature [14] or the angle between the incident H_2O beam and the surface [21] play a role in the amorphous nature of the sample.

There are numerous results in the literature concerning the physical properties of amorphous ice, but there seems to be little agreement between the experiments. For example, Sivakumar et al. [22] have found that amorphous ice can be prepared with substrate temperature as high as 110 K: under such conditions, their Raman spectra are similar and independent of temperature; conversely Ghormley [23,24] – using volumetric techniques – and Hagen et al. [25] – using infrared spectroscopy – have found that amorphous ice at 10 K is in a metastable form which undergoes an irreversible transformation to a more ordered form of amorphous ice upon warm up. This is in agreement with the results of X-ray diffraction from Narten et al. [26] who have shown that there are two different amorphous ice phases depending on the substrate temperature (10 or 77 K), and this has been also confirmed by Jenniskens and Blake [4]. On the other hand, for Olander and Rice [27], ices prepared at 77 K and higher temperatures contain considerable pre-crystalline parts. Furthermore, there is little agreement on the time scale involved in the crystallization: from a few seconds at about 150 K [28,29] to 18 min at 135 K [25,30] and even 45 min at 155 K [31]. Dowell and Rinfret [32] have shown that crystallization rate strongly depends on temperature.

Disagreements can also be observed with studies concerning surface characterization using N_2 adsorption isotherms: the values obtained for the heat of adsorption

* Corresponding author.
E-mail address: proubin@piima1.univ-mrs.fr (P. Roubin).

0301-0104/$ - see front matter © 2004 Elsevier B.V. All rights reserved.
doi:10.1016/j.chemphys.2004.01.008

are similar for all the published results whereas those for the specific surface area vary from 11.8 to 400 $m^2\ g^{-1}$ [13,14,33,34]. The main contribution to this type of measurements comes from Mayer and Pletzer [14,34] who have attributed the high magnitude of the specific surface area of amorphous ice to the presence of micropores (i.e., pores having dimensions less than 2 nm). The hypothesis of a microporous structure has also been analyzed by X-ray spectroscopy [35].

Disagreements can be explained by considering that amorphous ice properties depend on the way ice is prepared, and also that results depend on the technique used for measurements. It is therefore advisable to use at least two techniques simultaneously to study and characterize amorphous ice. This permits the correlation of different types of data and can therefore overcome some of the technical limitations. Our experimental setup allows us to simultaneously record spectroscopic and volumetric data. We have already shown that we can correlate the two techniques by plotting what we call infrared isotherms (i.e., the evolution in the integrated absorbance of selected infrared bands versus the relative pressure), in order to estimate the adsorption energies and to determine the surface or non-surface nature of the infrared signals [36,37]. Here we focus our attention on the modifications in surface structure induced by annealing, and we re-investigate amorphous ice porosity. This paper is organized as follows: experimental methods and models are detailed in Section 2; results from both techniques and discussion concerning the characterization of the ice sample, annealing-induced modifications and porosity are included in Section 3; Section 4 is devoted to concluding remarks.

2. Experimental

Volumetric isotherms and infrared measurements were simultaneously performed on a single sample in a closed copper cell provided with two sapphire windows, the experimental set-up and the way of preparing ice being described in detail in previous papers [36,37]. In brief, we used distilled water which was degassed at 10^{-7} mbar in successive freeze–thaw cycles, and then sealed under vacuum. A gas mixture H_2O:Ar (1:30) was promptly sprayed (rate of water molecules: $\approx$0.01 mol h^{-1}) in the cell maintained at 40 K under a vacuum better than 10^{-6} mbar. To eliminate argon, the sample was then pumped and slowly annealed (0.2 K min^{-1}) for about 5 h to 90 K. This annealing is limited, inducing no crystallization of ice, and therefore the sample will be considered as *without annealing* in what follows. Gas introduction was at the bottom of the cell and the ice sample looked like a vertical column through the cell, not much ice being on the cell windows. It was then not possible to have the value of its thickness; we estimated the gas amount that we introduced in order to obtain OH stretching absorbance less than unity and therefore to deduce quantitative information from infrared data. The temperatures were determined by measuring the saturation pressure p^0 of the gas and using the Clapeyron's law. The infrared spectra were collected using a Nicolet 7199 FTIR spectrometer. The resolution was 1 cm^{-1}, and 200 scans were collected per spectra.

We performed point by point isotherms: for each point of the isotherm, we collected the value of equilibrium pressure p to quantify the adsorbed amount, and we recorded an infrared spectrum to obtain the alterations in the signals of both ice and adsorbate, provided that the latter had an infrared active mode. The adsorption isotherm was finished when saturation pressure p^0 ($\sim$24.2, 10.0, 7.1 and 5.6 mbar, respectively, for N_2, CO, Ar and CH_4) was reached (i.e., the 3D phase was formed). Uncertainty in pressure measurements was less than 1.5×10^{-3} mbar and this led to an error bar for the adsorbed amount smaller than the size of the symbols used to plot isotherms. At the end of the experiment, the adsorbate was desorbed. We checked that the ice surface had not been perturbed during adsorption by comparing the infrared spectra of bare ice, before and after adsorption, and by re-performing an isotherm of a gas used as a reference. The adsorbed amounts were similar for a given equilibrium pressure, showing that the ice surface had not been irreversibly altered during adsorption.

N_2 is widely used to probe surfaces and we have compared our results with those already published [13,14,23,33,34] to validate our method. To compare the adsorption of various gases in similar conditions [38,39], N_2 was adsorbed at 56 K; though it is 21 K lower than the temperature usually used with N_2 (77 K), its mobility is still great enough to allow diffusion at the sample surface. In addition, this prevents a large saturation pressure above the sample which may warm and perturb the ice surface.

We used the Brunnauer, Emmet and Teller (BET) model [40] to determine the monolayer capacity v_m, the BET constant C and also the net heat of adsorption $E^a - E^c$ which represents the difference between the adsorption energy and the condensation energy. v_m and C are two parameters which can be determined by plotting the linear transformed BET equation: $p/[v^a(p-p^0)] = f(p/p^0)$, v^a being the volume of the gas adsorbed on the surface. $E^a - E^c$ and the relative pressure at monolayer completion $(p/p^0)_m$ can be estimated using the following relations: $E^a - E^c = RT \ln C$, and $(p/p^0)_m = 1/(\sqrt{C}+1)$. C and $(p/p^0)_m$ give information on the strength of the interactions between the adsorbate and the surface: the lower $(p/p^0)_m$, the larger C, and the stronger the interactions. The calculated values of $E^a - E^c$ are indicative only, but are useful to compare experiments performed at different temperatures. The accuracy of v_m and $E^a - E^c$

has been determined for each isotherm; the values of a are given $\pm 4\%$ and those of $C \pm 9\%$, which leads to values of $E^a - E^c \pm 0.2$ kJ mol^{-1}. According to the results obtained on various materials [41], the fit of the linear transformed BET equation is relevant in a small range of relative pressure only ($0.05 < p/p^0 < 0.35$ in the case of N_2). For each adsorbate, BET values were then calculated being very careful to achieve consistency of pressure range used for fitting data points.

Concerning the analysis of porosity, we used a "α-plot" method [41] which is an empirical method allowing a semi-quantitative analysis of microporosity. Basically, it uses standard data obtained on a non-porous chemically equivalent reference material, and consists in plotting the amount adsorbed on the sample versus that adsorbed on the reference under the same conditions. If the sample is also non-porous, the adsorption is similar on both materials and the adsorbed amounts are proportional: the plot is a straight line. Conversely, for a microporous sample, a deviation from linearity at the beginning of adsorption is observed: the expected enhanced interaction for molecules confined in micropores leads to an enhanced adsorbed amount. After the micropore filling, the adsorption occurs on the external surface (i.e., non-microporous surface) and the plot is merely a straight line. The specific surface area of the external surface can be estimated from this linear part, giving an estimation of the relative weight of the microporous and non-microporous surfaces.

3. Results and discussion

3.1. Characterization of the ice sample

3.1.1. Adsorption isotherm volumetry

More than 25 samples of amorphous ice have been characterized, using N_2 as the probe molecule. The adsorbed amount is plotted as a function of the relative pressure p/p^0 (square) in Fig. 1 for a typical isotherm (56 K) obtained for a typical sample. According to the IUPAC classification [41], it is type II: in the first part, v^a rises sharply at low values of p/p^0 and this corresponds to monolayer completion; the second part – roughly linear – corresponds to multilayer growth, and the third part (not shown here), where v^a rises sharply again when

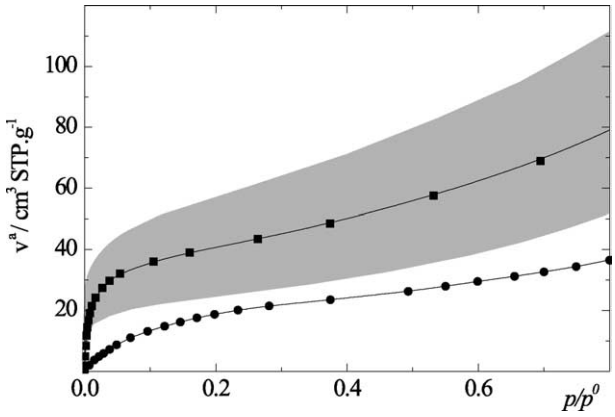

Fig. 1. N_2 (■) and CH_4 (●) adsorption isotherms on amorphous ice, respectively, at 56 and 73 K; the grey zone indicates the range probed by N_2 isotherms on the whole series of samples.

p/p^0 tends to 1, corresponds to condensation (i.e., the solid is formed above the adsorbed amount). The grey area in Fig. 1 represents the whole adsorbed volume that we have probed: the limit on the top (respectively the bottom) of this area is the isotherm obtained on the sample with the largest (respectively the smallest) specific surface area.

We have obtained large specific surface areas typically between 95 and 220 m^2 g^{-1}, using the value of N_2 cross-sectional area at 77 K (0.162 nm^2). These values (Table 1) are in good agreement with earlier results [13,14,23,33,34], as is the type II shape found for the isotherms. The distribution of the values of specific surface area is similar to that observed in the work of Schmitt [13] (Table 1) and is probably due to variations in the method used for ice preparation. Generally speaking, amorphous ice is expected to present a larger specific surface area if water vapor is deposited faster. In our case, the deposition rate is not precisely controlled (roughly estimated between 0.04 and 0.14 mol h^{-1}) and we did not manage to find a direct relation between deposition rate and specific surface area. We have also determined the net heat of adsorption $E^a - E^c$ using the BET theory, and found values between 2.3 and 2.6 ± 0.2 kJ mol^{-1}, in agreement with values already published [13,14,23,34,42]. We would like here to emphasize that, despite differences in the way of ice was prepared, we have obtained the same shape of isotherms and the same values of both specific surface area and net heat of

Table 1
Specific surface area a/(m^2 g^{-1}), BET constant C and net heat of adsorption $E^a - E^c$/(kJ mol^{-1}) determined using the BET theory at temperature T/K

Sample	T	a	C	$E^a - E^c$
Mayer and Pletzer [14]	77	356–421	18–30	1.8–2.2
Schmitt [13]	77	34–290	41–50	2.4–2.5
Ghormley [23]	77	213–241	83–121	2.8–3.1
Nair and Adamson [33]	77	34	85	2.8
This work	56	95–315	140–230	2.3–2.6

adsorption as previous works devoted to amorphous ice: this proves that these ice samples can be compared, and that they have similar interactions with N_2.

To probe the ice surface, we have also used CH_4, a spherical molecule (cross-sectional area 0.177 nm^2) supposed to have no specific interaction with the surface. Fig. 1 displays a typical CH_4 isotherm: it is also type II, the comparison of the shape of the two isotherms having already been detailed elsewhere [39]. It should be noted that the ratio of the adsorbed amounts at monolayer completion $v_m(N_2)/v_m(CH_4)$ is 1.33, whereas the ratio of the distances between the nearest neighbors in the solid is only 1.09. This indicates that the ice surface allows the N_2 adlayer to have a specific geometry which leads to an adsorbed phase with a greater density than that of CH_4. It has been already shown that N_2 can stand perpendicular to surfaces [43,44], and its cross-sectional area, usually estimated at 0.162 nm^2, can therefore be reduced to 0.112 nm^2 [41]. In fact, when taking CH_4 as a reference, we obtain for N_2 an intermediate value for the effective cross-sectional area (0.133 nm^2), indicating the possibility of various orientations of the molecule on the surface. This has been confirmed in the case of CO by calculations [37] where the geometry of the adlayer has been determined, and it has been shown that the specific L-type quadrupole–quadrupole interactions lead to a high density of the adlayer.

3.1.2. Infrared spectroscopy

There are numerous contributions to the vibrational spectroscopy of ice which show that this technique is well suited to study ice modifications. For example, Mayer and Bruggeller [12] have proved that infrared spectra show variations depending on the way the sample is prepared, and Hagen et al. [25] have proved that moderate resolution spectra can provide information on the thermal history of water condensed on cold interstellar dust grains. Furthermore, several works [38,39,42,45–50] have shown that infrared spectroscopy is a good technique to study amorphous ice surface and adsorption phenomena. We have used this technique and compared our spectra with those already published, to make sure of structure and phase of our samples. In fact, the infrared spectrum obtained after annealing at 90 K and cooling to 56 K (Fig. 2(a), lower curve) compares well with previously published details on spectra of amorphous ice [19,42,51,52]. The amorphous nature is characterized first, by the shape of the broad band centered at roughly 3250 cm^{-1} (OH stretching motions of bulk molecules linked through the strong hydrogen bond network), and second, by the weak band at 3696 cm^{-1} (low-coordinated surface molecules with a dangling OH bond – dH molecules – [16]). We have also been able to detect the two other surface modes previously characterized by Devlin et al. [42,53], originating from the three-coordinated molecules with a free

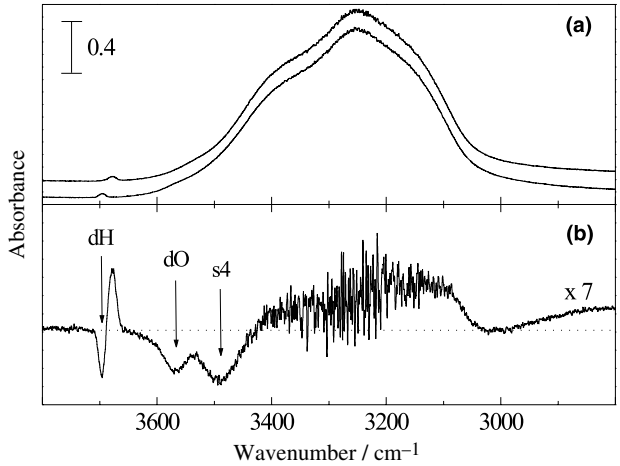

Fig. 2. (a) Infrared spectra of bare ice at 56 K (lower) and of ice covered by a monolayer of N_2 at 56 K (upper); and (b) difference spectrum (upper) – (lower).

electron pair on oxygen atom – dO molecules – and from the four-coordinated molecules with a distorted H bond tetrahedron – s4 molecules –, their positions being, respectively, measured here at 3549 and 3503 cm^{-1}. The dH band is clearly observed outside the broad band at 3250 cm^{-1} (FWHM 250 cm^{-1}), whereas these latter surface bands can be detected only by difference, after annealing or after using a probe molecule: Fig. 2(a) shows the spectrum of bare ice (lower curve) and of ice covered by a N_2 monolayer (upper curve), and Fig. 2(b) shows the difference between the two spectra, bare ice being taken as the reference. We have plotted the infrared isotherms of the three negative bands and have checked that they are type I [39]: this is in agreement with their assignment to the three modes of the ice surface, and this indicates that N_2 is interacting with all three surface sites. We have also checked using infrared spectroscopy that after desorption of the probe molecule (i) there is no more adsorbate on the ice surface and (ii) the ice surface has recovered its original properties.

3.2. Annealing-induced modifications

3.2.1. Infrared data

In order to determine the temperature range of amorphous ice stability, the sample was slowly annealed to 190 K at a rate of 0.5 K min^{-1}, and the infrared spectra were collected at 5 min intervals during the annealing. Fig. 3 shows the infrared spectra recorded at $T = 40$, 90, 120, 140, 160 and 190 K. No change is observed between 40 and 90 K whereas above 105 K (not shown here), the three surface signals begin to decrease. The modifications induced by annealing to 130 K are highlighted by a difference spectrum shown in Fig. 3(g): the decrease in the three surface bands (indicated by arrows) is obvious, and the changes arising at lower

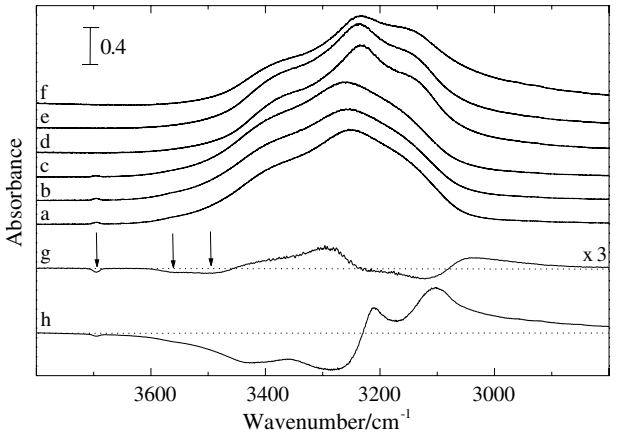

Fig. 3. Infrared spectra of bare ice at: (a)–(f) 40, 90, 120, 140, 160 and 190 K, and infrared difference spectra: (g) ice at 130 K minus ice at 40 K (the arrows indicate the surface bands), and (h) ice at 40 K having been annealed to 190 K minus ice at 40 K.

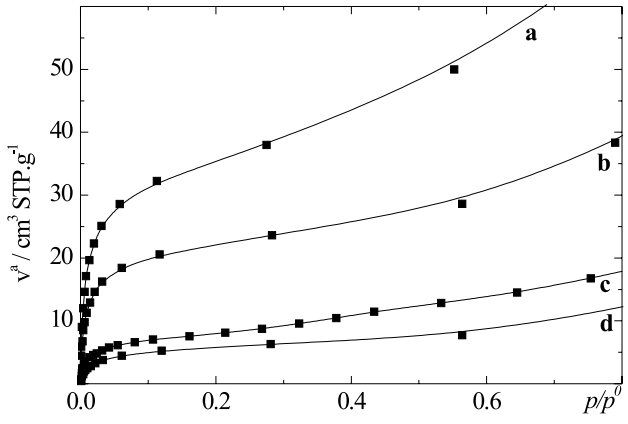

Fig. 4. N_2 adsorption isotherm at 56 K on amorphous ice: (a) without annealing, and annealed to (b) 120, (c) 140, and (d) 160 K.

frequencies for bulk vibrations correspond to a small blue-shift. It should be noted that this shift is reversible and is thus probably due to thermal effects. Conversely, the modifications induced by annealing to 190 K, highlighted on Fig. 3(h) by a difference spectrum, are non-reversible and indicate a transfer from high-frequency (low coordinated molecules) to low-frequency (high coordinated molecules). At 140 K, there is no more surface signal; the main band is 15 cm^{-1} redshifted and a new shoulder appears at 3150 cm^{-1}, indicating that the bulk has crystallized. By following the shift of the main band we obtain a value of 137.5 ± 2 K for the transition, in good agreement with values already published by Jenniskens and Blake [4]: according to these authors, ice becomes cubic. No major change is observed between 140 and 160 K, whereas above 160 K the shoulder at 3150 cm^{-1} increases, probably due to the formation of hexagonal ice. The heating rate was remained low and constant during the whole annealing: we can therefore clearly distinguish between (i) the reorganization of the ice structure which is shown by the decrease in the surface dH signal and which occurs within a large temperature range (105–130 K), and (ii) the crystallization which is shown by the shift in the bulk stretching OH signal and which occurs at ~137.5 K.

3.2.2. Specific surface area

Taking the modifications of the infrared spectrum into account, we chose four conditions of amorphous ice to perform N_2 isotherms at 56 K: without annealing, and after annealing to 120, 140 and 160 K. The measurements were performed on several samples to check that an annealing–cooling cycle does not disturb subsequent annealing. In what follows, ice annealed to 160 K will be taken as the reference for crystalline ice.

Fig. 4 shows the N_2 isotherms that we have performed at 56 K after the various annealing–cooling cycles, all type II. We have used the BET theory to determine adsorbed amount at monolayer completion v_m, specific surface area a, and net heat of adsorption $E^a - E^c$ (Table 2). Specific surface area dramatically decreases when the sample is annealed to 140 K. The sample loses nearly 33% (respectively 80%) of its area when annealed to 120 K (respectively 140 K) while it remains at roughly 20% of its initial value from 140 to 160 K. For $T < 140$ K, the decrease in specific surface area, caused by the loss of surface sites, actually follows the loss of dH surface signals observed on the infrared spectra.

No significant changes induced by annealing or crystallization have been observed in net heat of adsorption. This means that the surface sites have similar energies in both cases, showing that the interactions are similar for amorphous and crystalline ice. It should be noted that the BET fit gives a crude estimation of a mean value of net heat of adsorption and is probably not well suited to evaluate subtle modifications occurring in the case of weak interactions.

3.2.3. Discussion

In Fig. 5, we have plotted the modifications in three parameters: specific surface area a, integrated absorbance of the dH signal A_{dH}, and shift of the position of the main infrared band $\Delta\nu_{OH}$, as functions of temperature T. a and A_{dH} are normalized in order to compare

Table 2
Specific surface area a/(m^2 g^{-1}), BET constant C and net heat of adsorption $E^a - E^c$/(kJ mol^{-1}), determined using the BET theory at 56 K on different ice samples

Sample	a	C	$E^a - E^c$
No annealing	122 (0)	222	2.5
Annealing to 120 K	83 (32)	145	2.3
Annealing to 140 K	28 (77)	127	2.2
Annealing to 160 K	22 (82)	112	2.2

The loss of a (in %) is indicated in brackets.

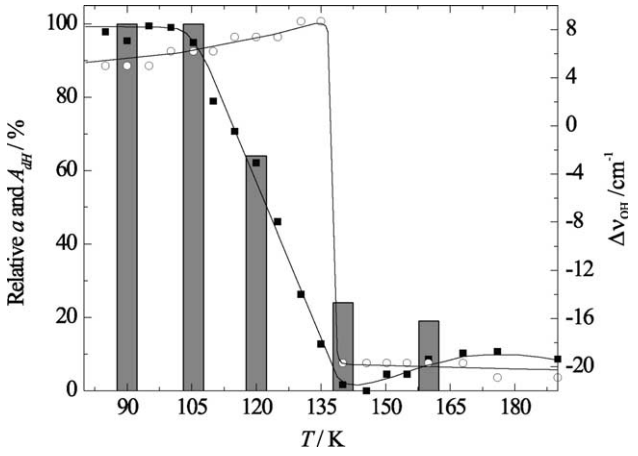

Fig. 5. Integrated absorbance of the ν_{dH} band A_{dH} (■), shift of the bulk stretching OH band $\Delta\nu_{OH}$ (○) and specific surface area a (bar) versus temperature T. Uncertainty is ~8% for a and 1 cm^{-1} for $\Delta\nu_{OH}$. For ν_{dH} it is ~10% for amorphous ice ($T < 135$ K) and reaches 100% for $T > 150$ K when the signal is very weak.

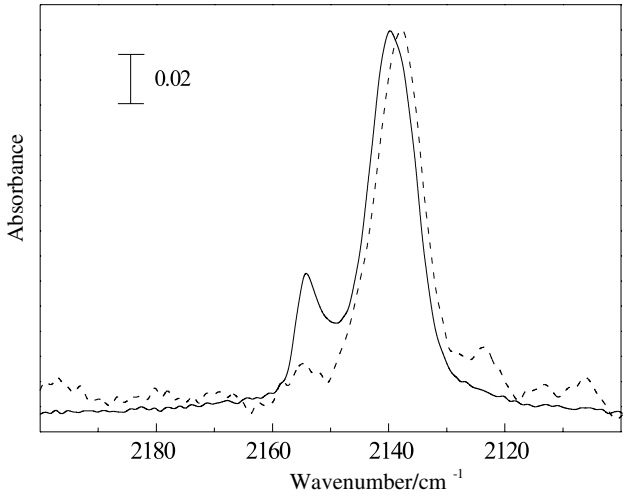

Fig. 6. Infrared spectra in the CO stretching region of CO adsorbed at 56 K (monolayer completion) on amorphous ice (continuous line) and crystalline ice (dashed line). The spectrum of crystalline ice has been scaled to get the same integrated absorbance of $\nu_{CO\text{-}2139}$ band. The relative intensities are 17, roughly corresponding to the relative specific surface areas.

them on the same scale; both are surface sensitive parameters whereas $\Delta\nu_{OH}$ is bulk sensitive. For $T < 105$ K, there is no change in either a or A_{dH}, the surface of amorphous ice being stable in this temperature range. The main band is weakly blue-shifted, due to a reversible thermal effect. From $T > 105$ to $T \sim 140$ K, the two surface signals slowly decrease, whereas $\Delta\nu_{OH}$ remains roughly constant, only showing a sharp modification at $T = 137.5 \pm 2$ K. This confirms the existence of two successive and distinct phenomena: first the re-organization of the whole ice structure leading to a lowering of the specific surface area, and second the crystallization of the ice leading to a long range ordering of the H bond network.

For $T > 145$ K, A_{dH} is close to zero, the values measured for $T > 165$ K for the band area being within noise. Conversely, a is roughly 20% that of amorphous ice and remains clearly not zero at $T = 160$ K. Our experimental uncertainties on both types of measurement allow us to conclude that A_{dH} and a decrease in the same manner for $T < 140$ K, whereas A_{dH} decreases more rapidly than a for $T > 140$ K, indicating a modification in the surface sites at crystallization. To look at this point more closely, we performed adsorption measurements on amorphous and crystalline ice using CO. In previous studies [19,37,54–57], it has been shown that CO adsorbed on amorphous ice presents two infrared bands at 2139 and at 2154 cm^{-1} which for clarity we call here $\nu_{CO\text{-}2139}$ and $\nu_{CO\text{-}2154}$. The former is close to that of solid CO and comes from first dO and s4 sites at the beginning of adsorption, then from multilayer formation, while the latter is blue-shifted and is attributed to CO interacting with dH sites only. Since this band is more intense than ν_{dH}, it can be used to probe the presence of dH sites. Fig. 6 shows the infrared spectra of CO adsorbed on amorphous and crystalline ice at 56 K. The whole signal of CO adsorbed on crystalline ice is lower than that on amorphous ice, in agreement with the lowering of specific surface area with annealing. We have scaled these spectra to get the same integrated absorbance for the $\nu_{CO\text{-}2139}$ band. If the ratio of the intensities of the two bands was the same for amorphous and crystalline ice, we should measure a $\nu_{CO\text{-}2154}$ signal and this is clearly not the case: there is less dH sites compared to the other sites for crystalline ice than for amorphous ice. This is in agreement with the lowering of A_{dH} which is larger than that of a at crystallization (Fig. 5), and is consistent with an increase in the water molecule coordination induced by allowing ice to reorganize with temperature. The dH signal can therefore be used as a surface probe for ice, but with care if used for a quantitative estimation when going from amorphous to crystalline ice.

3.3. Porosity of the sample

3.3.1. Microporosity

Our first analysis of the amorphous ice microporosity has been published previously [58] and we add here new experimental results. Amorphous ice is always thought of as a microporous material, the main reference for this assessment being the work of Mayer and Pletzer [14,34]. They have shown this by comparing the adsorption capacity of N_2 on amorphous ice and that on crystalline ice, plotting the first versus the second (so-called hereafter α-plot). We have shown that care must be taken in analyzing this type of data, especially when using N_2 as the probe molecule for specific surface area

measurements, and that our ice samples are not microporous. Fig. 7 shows the α-plots for four gases – N_2 and CO at 56 K, CH_4 at 73 K and Ar at 60 K – and two different ice samples – sample 1 having a specific surface area of 110 $m^2\ g^{-1}$ when amorphous and sample 2 having a specific surface area of 160 $m^2\ g^{-1}$ when amorphous. In all the cases, the reference is ice annealed at 160 K: this ice has been shown to be stable at this temperature and therefore is a good sample of crystalline ice. We can in addition assume that this ice is non-microporous, its specific surface area being too low to originate from the internal surface of micropores.

Fig. 7(a) and (b) show the different behaviors observed for N_2, CH_4 and Ar on sample 1. The deviation from linearity that we observed in the case of N_2 (Fig. 7(a)) before monolayer completion has been previously observed by Mayer and Pletzer and assigned to the presence of micropores [14]. On the contrary, using CH_4 or Ar, we show here that a straight line fits the data (Fig. 7(b)), the slope of the line being roughly equal to the ratio between the specific surface areas of amorphous and crystalline ice. It should be noted here that the slight deviation to straight line that is observed is due to the process used to calculate the data: in fact, in this type of plot, interpolation is done to get the adsorbed volumes at the same pressure for both amorphous and crystalline ice, though this is generally not the case for the experimental data. This deviation from a perfect straight line is however well distinct to that appearing at the first steps of the adsorption. We thus believe that the non-linearity observed in the case of N_2 is not due to micropores because it should not be dependent on the probe gas. In fact, the three adsorbates have similar diameters (0.45, 0.42 and 0.47 nm for N_2, Ar and CH_4, respectively) and if micropores are probed by N_2, they should be probed by CH_4 and certainly by Ar which is smaller than N_2. We have therefore tested the adsorption of CO which is similar to N_2 and have obtained similar deviation from linearity for the two gases on sample 2 (Fig. 7(c)). Analogous results are obtained for the same sample of ice annealed at 120 K (Fig. 7(d)): this ice is intermediate between amorphous and crystalline ice, having already lost surface sites, and the curves therefore have smaller slopes due to the smaller ratio between their specific surface areas. It should be noted that, as seen in both Figs. 7(c) and (d), the effect is slightly larger for CO than for N_2.

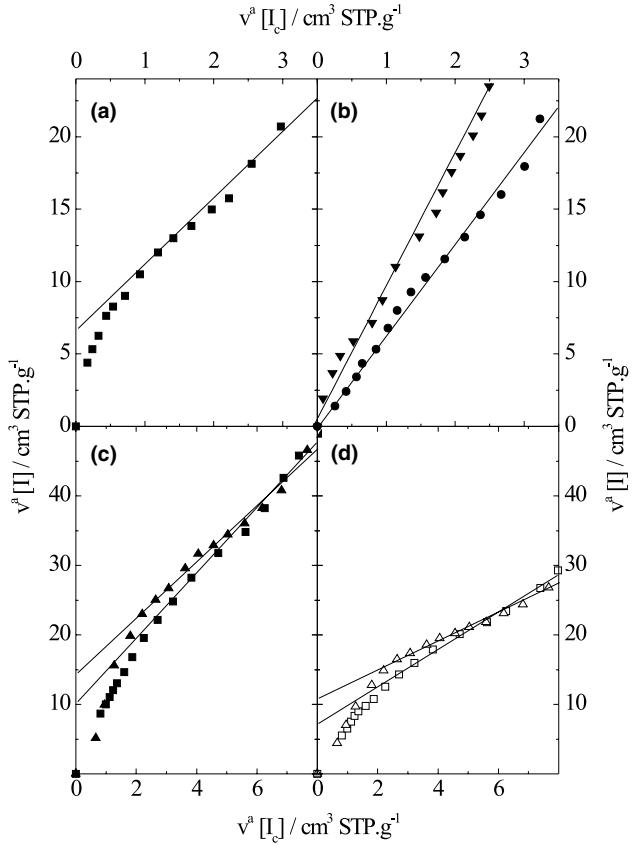

Fig. 7. α-plots: correlation between the adsorbed amounts measured on ice v^a [I] and those on crystalline ice v^a [Ic] (a) N_2 at 56 K (■) on a ice sample having a 110 $m^2\ g^{-1}$ surface specific area when amorphous, (b) CH_4 at 73 K (▼) and Ar at 60 K (●) on the same sample as (a), (c) N_2 (■) and CO (▲) at 56 K on a ice sample having a 160 $m^2\ g^{-1}$ surface specific area when amorphous, (d) the same as (c) for ice annealed to 120 K. The straight lines are guides for the eye.

We will now discuss the possible origin of the deviation from linearity observed in the case of N_2 and CO: we have already observed a specific behavior for both CO and N_2 when comparing the adsorption of these two molecules with that of spherical adsorbates [38,39] and we have shown for the former a weak hydrogen bonding with the dH sites. A closer study on CO adsorption [37] has shown that the adsorbed CO molecules can interact in a L-type configuration above a pair of dH and s4 water molecules because of quadrupolar interactions, stabilizing the linear dH:CO configuration with CO perpendicular to the surface. The dH sites are thus expected to interact more strongly with CO and N_2 than the other surface sites, and are expected to be the sites first occupied during adsorption. We have shown in Section 3.2 that the ratio between the numbers of the surface molecules of the different types is not the same for amorphous and crystalline ice: the dH molecules are less numerous on crystalline ice. This can thus explain the deviation from linearity which we have observed: the first part of the curve has a higher slope than the second part and corresponds to the adsorption on the dH sites: the higher slope is thus merely due to the higher ratio between the dH surface sites on the two ices. Moreover, the quadrupole moment of CO (-9.47×10^{-40} C m^2) is larger than that of N_2 (-4.65×10^{-40} C m^2): the effect is thus expected to be larger for CO than for N_2, in agreement with what is observed in Fig. 7. The α-plot non-linearity is therefore caused by the existence of specific interactions, and not by the existence of

micropores. A comparable study has already shown that the N_2 adsorption on a hydroxylated silica is influenced by specific interactions between N_2 and the surface hydroxyl groups [59], and the work of Storck et al. [60] concerning other surfaces has led to similar conclusions about the special behavior of N_2.

Another indication of non-microporosity is given by the shape of the step: a microporous sample should give rise to a much sharper step which appears with an inflection point in the logarithmic plot of the isotherm [60], and this is clearly not the case for this type of sample [58]. The shape of the step is related to adsorption energy: the values obtained for ice (Table 1) are clearly too low to be consistent with a confinement in micropores, which would lead to an enhancement of attractive interactions, due the walls. Moreover, in all our experiments the whole amount adsorbed was easily desorbed merely by expanding the gas contained in the cell into vacuum, confirming the absence of micropores.

3.3.2. Mesoporosity and macroporosity

We now look at the origin of the large specific surface area of our samples. Like Mayer and Pletzer [14], we found no evidence for hysteresis loops during desorption (Fig. 8(a)), which would have validated the hypothesis of mesoporosity; such reversible type II isotherms are typical of those produced by non-porous or macroporous solids. On the contrary, Schmitt et al. [61] have measured a hysteresis loop for high relative pressure ($p/p^0 > 0.4$), attributed to the capillary condensation in mesopores. This puts the stress on the crucial role played by the preparation conditions in the final ice structure. For example, a low temperature deposition as well as the use of a carrier gas are known to favor an amorphous character of ice and a high adsorption capacity [14,34,61–63]. On the other hand, ice has a surprisingly low adsorption capacity after the monolayer completion: just before condensation ($p/p^0 \leqslant 1$), the surface coverage is only twice as large as than at monolayer completion. Macroporous samples are expected to have a much larger adsorption capacity, and therefore we think that our samples are neither mesoporous nor macroporous.

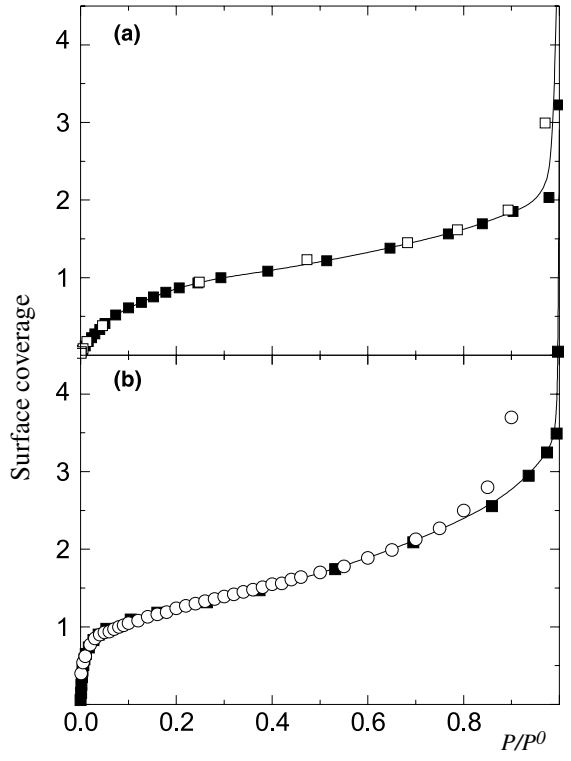

Fig. 8. (a) CH_4 surface coverage (v^a/v_m) on amorphous ice at 73 K showing the adsorption (■) and the desorption (□), (b) N_2 surface coverage on amorphous ice at 56 K (■) and on non-porous silica TK8000 [41] (○) at 77 K versus relative pressure p/p^0.

We have also compared our isotherm measurements with those performed by Payne et al. [59] on samples of silica. Fig. 8(b) shows N_2 surface coverage versus relative pressure for our sample of ice at 56 K and for silica TK800 at 77 K which was found to be non-porous and to consist of discrete spherical particles. Both isotherms totally correspond up to $p/p^0 = 0.8$, meaning that adsorption occurs on amorphous ice in the same way as it occurs on this non-porous silica. It should be noted that the surface of this silica contains hydroxyl groups, adding some analogy with the surface of ice. For $p/p^0 > 0.8$, the adsorbed amount is larger in the case of silica, which may be due to inter-particle condensation.

Our results are thus consistent with the hypothesis of samples constituted by grains and inter-grain cavities. Mixing H_2O with argon during vapor deposition probably does not prevent the clustering of water molecules due to strong attraction via hydrogen bonding, these clusters then being the nucleus for condensation of grains. We have used the simple model of an assembly of spherical grains to determine the grain diameter $d = 6/\rho a$. Taking $\rho = 0.91$ g cm^{-3} [26] and $a \geqslant 100$ m^2 g^{-1} leads to $d \leqslant 70$ nm. During annealing, the grains collapse and form larger grains which diameter could be larger than 300 nm.

4. Conclusion

Results combining both infrared spectroscopy and adsorption isotherm volumetry have been presented, giving new data for characterizing amorphous and crystalline ice structures. The main features are summarized here:

1. Two distinct steps in the warm up of ice have been revealed: first the re-organization of the whole ice structure by collapsing from 105 to 140 K, and second the actual crystallization phenomena at 137.5 ± 2 K.

2. The comparison of crystalline and amorphous surface sites have shown that the dH sites (dangling OH bonds) are more numerous than the other sites on the latter, indicating a higher rate of coordination for water molecules on crystalline ice surface.
3. CO has revealed a good tool for probing the ice surface structure, giving a dH sensitive signal at 2154 cm^{-1} easier to detect than the dH signal alone. This could perhaps be used to estimate the presence or the absence of amorphous ice in icy grains for suitable regions of the interstellar medium. Moreover the ratio between this signal and that of CO at 2139 cm^{-1} may give information on the ratio of surface sites, and therefore on the history of the ice.
4. Our ice samples are clearly amorphous *and* non-microporous. This may be not the case for all the amorphous ice samples, ice structure strongly depending on experimental conditions. The point here is that care must be taken when probing microporosity with adsorption methods because N_2 adsorption is not well suited.

Finally, we would like to emphasize that ice can have a large specific surface area and at the same time still be non-microporous. The adsorption capacity is nevertheless similar to that measured on previously supposed microporous samples, leading to similar gas storage ability. On the other hand, a non-microporous structure prevents efficient trapping in the pores, and gives greater probabilities of diffusion, collision and reactivity between adsorbates. We believe that this is of interest in understanding the chemical reactivity occurring in the icy grains of the interstellar medium.

References

[1] R. Smoluchowski, Science 201 (1978) 809.
[2] A. Léger, J. Klein, S.D. Chevigne, C. Guinet, D. Defourneau, M. Belin, Astron. Astrophys. 79 (1979) 256.
[3] B. Schmitt, Molecules and Grains in Space, 50th International Meeting of Physical Chemistry, Mt Saint-Odile, France, 1993.
[4] P. Jenniskens, D.F. Blake, Science 265 (1994) 753.
[5] A.G.G.M. Tielens, W. Hagen, J.M. Greenberg, J. Phys. Chem. 87 (1983) 4220.
[6] T.Y. Brooke, A.T. Tokunaga, H.A. Weaver, J. Crovisier, D. Bockelee-Morvan, D. Crisp, Nature 383 (1996) 606.
[7] V. Buch, J.P. Devlin, Molecules in Astrophysics: Probes and Processes, Kluwer academic publishers, 1997, p.321.
[8] R.L. Hudson, M.H. Moore, Icarus 126 (1997) 233.
[9] M.H. Moore, R.L. Hudson, Icarus 135 (1998) 518.
[10] M.P. Bernstein, S.A. Sandford, L.J. Allamandola, J.S. Gillette, S.J. Clemett, R.N. Zare, Science 283 (1999) 1135.
[11] O. Mishima, L.D. Calvert, E. Whalley, Nature 310 (1984) 393.
[12] E. Mayer, P. Bruggeller, Nature 298 (1982) 715.
[13] B. Schmitt, Ph.D. thesis, Université scientifique technologique et médicale, Grenoble (Novembre, 1986).
[14] E. Mayer, R. Pletzer, Nature 319 (1986) 298.
[15] G. Ritzhaupt, N. Smyrl, J.P. Devlin, J. Chem. Phys. 64 (1976) 435.
[16] V. Buch, J.P. Devlin, J. Chem. Phys. 94 (1991) 4091.
[17] B. Rowland, M. Fisher, J.P. Devlin, J. Chem. Phys. 94 (1991) 812.
[18] A. Givan, A. Loewenschuss, C.J. Nielsen, J. Chem. Soc. Faraday Trans. 92 (1996) 4927.
[19] A. Allouche, P. Verlaque, J. Pourcin, J. Phys. Chem. B 102 (1998) 89.
[20] S.B. Berland, D.E. Brown, M.A. Tolbert, S.M. George, Geophys. Res. Lett. 22 (1995) 3493.
[21] K.P. Stevenson, G.A. Kimmel, Z. Dohnalek, R.S. Smith, B.D. Kay, Science 283 (1999) 1505.
[22] T.C. Sivakumar, S.A. Rice, M.G. Sceats, J. Chem. Phys. 69 (1978) 3468.
[23] J.A. Ghormley, J. Chem. Phys. 46 (1967) 1321.
[24] J.A. Ghormley, J. Chem. Phys. 48 (1968) 503.
[25] W. Hagen, A.G.G.M. Tielens, J.M. Greenberg, Chem. Phys. 56 (1981) 367.
[26] A.H. Narten, C.G. Venkatesh, S.A. Rice, J. Chem. Phys. 64 (1976) 1106.
[27] D.S. Olander, S.A. Rice, Proc. Natl. Acad. Sci. USA 69 (1972) 98.
[28] J.A. McMillan, Nature 206 (1965) 806.
[29] R.H. Beaumont, H. Chihara, J.A. Morrison, J. Chem. Phys. 34 (1961) 1456.
[30] A.H. Hardin, K.B. Harvey, Spectrochim. Acta 229 (1973) 1139.
[31] S.A. Rice, M.S. Bergren, L. Swingle, Chem. Phys. Lett. 59 (1978) 14.
[32] L.G. Dowell, A.P. Rinfret, Nature 188 (1960) 1144.
[33] N. Nair, A. Adamson, J. Phys. Chem. 74 (1970) 2229.
[34] R. Pletzer, E. Mayer, J. Chem. Phys. 90 (1989) 5207.
[35] P. Parent, C. Laffon, C. Mangeney, F. Bournel, M. Tronc, J. Chem. Phys. 117 (2002) 10842.
[36] C. Manca, P. Roubin, C. Martin, Chem. Phys. Lett. 330 (2000) 21.
[37] C. Manca, C. Martin, A. Allouche, P. Roubin, J. Phys. Chem. B 105 (2001) 12861.
[38] C. Martin, C. Manca, P. Roubin, Surf. Sci. 502–503C (2002) 275.
[39] C. Manca, C. Martin, P. Roubin, J. Phys. Chem. B 107 (2003) 8929.
[40] S. Brunauer, P. Emmet, E. Teller, J. Am. Chem. Soc. 60 (1938) 309.
[41] F. Rouquerol, J. Rouquerol, K. Sing, Adsorption by Powders & Porous Solids, Academic Press, London, 1999.
[42] J.P. Devlin, V. Buch, J. Phys. Chem. 99 (1995) 16534.
[43] J. Rouquerol, F. Rouquerol, C. Prs, Y. Grillet, M. Boudellal, B. Imelik, Characterization of Porous Solids, London Society of Chemical Industry, 1979.
[44] J. Rouquerol, Y. Grillet, M.J. Torralvo, Fundamental of Adsorption, Engineering Foundation, New York, 1984.
[45] J. Sadlej, B. Rowland, J.P. Devlin, V. Buch, J. Chem. Phys. 102 (1995) 4804.
[46] L. Delzeit, M.S. Devlin, B. Rowland, J.P. Devlin, V. Buch, J. Phys. Chem. 100 (1996) 10076.
[47] J.P. Devlin, V. Buch, J. Phys. Chem. B 101 (1997) 6095.
[48] M. Rozenberg, A. Loewenschuss, Y. Marcus, Langmuir 15 (1999) 5454.
[49] A.B. Horn, M.A. Chesters, M.R.S. McCoustra, J.R. Sodeau, J. Chem. Soc. Faraday Trans. 88 (1992) 1077.
[50] C. Manca, A. Allouche, J. Chem. Phys. 114 (2001) 4226.
[51] W.G. Madden, M.S. Bergren, R. McGraw, S.A. Rice, M.G. Sceats, J. Chem. Phys. 68 (1978) 3497.
[52] J.P. Devlin, J. Sadlej, V. Buch, J. Phys. Chem. A 105 (2001) 974.
[53] B. Rowland, N.S. Kadagathur, J.P. Devlin, T. Feldman, M.J. Wojcik, J. Chem. Phys. 102 (1995) 8328.
[54] S.A. Sandford, L.J. Allamandola, A.M. Tielens, G.J. Valero, Astrophys. J. 329 (1988) 498.
[55] J.P. Devlin, J. Phys. Chem. 96 (1992) 6185.
[56] B. Schmitt, R. Grim, M. Greenberg, 22nd Eslab Symposium on Infrared Spectroscopy in Astronomy, Salamanca, Spain, 1988.
[57] M.E. Palumbo, J. Phys. Chem. A 101 (1997) 4298.
[58] C. Manca, C. Martin, P. Roubin, Chem. Phys. Lett. 364 (2002) 220.

[59] D.A. Payne, K.S.W. Sing, D.H. Turk, J. Colloid Interface Sci. 43 (1973) 287.
[60] S. Storck, H. Bretinger, W.F. Maier, Appl. Catal. A 174 (1998) 137.
[61] B. Schmitt, J. Ocampo, J. Klinger, J. Phys. Coll. C 1 (48) (1987) 519.
[62] W. Langel, A. Becker, H.-W. Fleger, E. Knözinger, J. Mol. Struct. 297 (1993) 407.
[63] E. Mayer, R. Pletzer, J. Chem. Phys. 80 (1984) 2939.